Asian Journal of Chemistry; Vol. 26, No. 19 (2014), 6370-6378

ASIAN JOURNAL OF CHEMISTRY

http://dx.doi.org/10.14233/ajchem.2014.16379

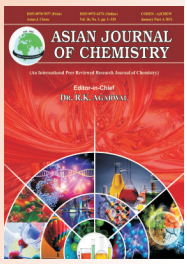

Effect of Supports on Stability and Water Tolerance of Co-Beta Based Catalysts in NO-SCR by CH_4

JIAQI CHEN[1,*], SHUWEI CHEN[2], RUIFENG LI[1,2] and JIAJUN ZHENG[2]

[1]Institute of Special Chemicals, Taiyuan University of Technology, Taiyuan 030024, P.R. China
[2]College of Chemistry and Chemical Engineering, Taiyuan University of Technology, Taiyuan 030024, P.R. China

*Corresponding author: Fax: +86 351 6010121; Tel: +86 351 6018384; E-mail: jinlchen@126.com

Received: 16 September 2013; *Accepted*: 12 February 2014; *Published online*: 16 September 2014; AJC-15920

The effect of supports on Co-Beta based catalysts was investigated by various characterizations and reactivity in the presence (2.5 % H_2O) and absence of vapor. As UV-visible, XPS, NO-TPD and NO-IR reported, the BZZ(Beta/ZSM5) and BMZ(Beta/MOR) composite supports boost the dispersion of Co active metal and decreased the BE value of catalyst, with a better acidity and stronger adsorption capacity expressed. Under dry condition, stronger stability on CoH-BZZ upon aged for 140 h was described compared with the one on CoH-Beta and CoH-BMZ. Under wet condition, both CoH-BMZ and CoH-BZZ catalysts exhibited higher catalytic activity, when the maximum NO conversion was 45 % on CoH-BMZ or 37 % on CoH-BZZ compared with 23 % on CoH-Beta. However, they had higher depression of NO conversion than CoH-Beta did in the presence of vapor. The loss of the active sites and the migration of active sites from Co^{2+} to cobalt oxide lead the deactivation of the catalysts.

Keywords: CoH-BZZ, CoH-BMZ, NO-SCR, Polarization, Deactivation mechanism.

INTRODUCTION

The nitrogen oxides (NO_x) exited from the combustion of biomass and fossil fuels are the source of severe environmental problems. For the past thirty years great effort were made in the research directed to find solutions for the NO_x problem. NH_3 (SCR) and the three-way catalyst (TWC) are two main methods for the removal of NO_x from emission gases. However, some serious drawbacks occurred, such as the ammonia slip, equipment corrosion, plugins, transport through residential areas on NH_3-SCR[1,2] and low NO reduction efficiency in the excess of O_2 on TWC[3,4]. Anyway, alternatively selective catalytic reduction of NO_x using hydrocarbons as reductant (HC-SCR) is currently attracting a great deal of interest for lean burns system.

Since two decades ago, selective catalytic reduction of NO by hydrocarbons had been widely investigated after the initial reports by Armor[5] and Capek *et al.*[6]. Co-zeolites (ZSM-5, mordenite and ferrierite mainly) were of particular interest because of their activity and selectivity when using methane[7]. Beta was another prevail support for NO-SCR by hydrocarbons except methane. Moreover, since the huge amount of water presented at the exhaust gas[8], the water insistence of the catalysts in the simulated exhaust gas atmosphere was very important and it was also the primary limitation for many zeolite based catalysts. Herein, both the stability and water tolerance were affected by different supports of the catalysts.

Most of the catalysts can maintain the activity steady in a long reaction time under dry condition. Besides, the mechanism of the decline of activity was simple. It was considered to be the dealumination, *i.e.*, removal of the tetrahedral Al^{3+} ion from the zeolite lattice, formation of metal oxides, loss of the dispersion and migration of exchanged cations to highly coordinated non-accessible locations[9-12]. It had been reported that deactivation by dealumination was slower for small than for large crystal size Co-MFI samples[13].

Under wet condition, it was basically concluded that exposure to water vapor at high temperatures irreversibly depre-sses the activity because some structural changes occur in the solids. The most important ones were dealumination[9,14]. Moreover, their catalytic activity was also strongly inhibited by the coexistence of water vapor, which was a serious concern for the development of these materials for practical purposes[15,16]. It was found that the effect of water vapor on CH-SCR activity greatly depends on Co^{2+} exchange level and the coexisting cation. The inhibiting effect of water can be explained by the competitive adsorption between H_2O and reactant[15-18]. However, it was found that the presence of water vapor remarkably enhanced the catalytic activity for C_3H_8-SCR over Co-MFI zeolite prepared from H-MFI zeolite, but inhibited the C_3H_8-SCR reaction over excess co-exchanged MFI and Co-Na-MFI prepared from Na-MFI zeolite[6]. Thus it must be the surface structure of supports which impacted the active sites surroundings and continuously changed the function of water in the

reaction system. Nevertheless, it was tested that the hydrothermal treatments resulted in significant modifications in the amount and distribution of metal species, namely an increase of Co oxides and Co-oxo species, simultaneously with the preservation of bare Co^{2+} cations[19].

Hence, the stability of the catalysts in the presence or absence of water was mostly significant and it was also complex for the deactivation under this condition. It is worth noticing these differences among the Co^{2+} active sites on different supports and their effects on water vapor in this system. The present paper was then took a contribution of the effect of supports CoH-Zeolite [Beta, BZZ (Beta/ZSM5), BMZ (Beta/MOR)] on the NO-SCR by CH_4 to resolve these questions.

EXPERIMENTAL

The composites, BZZ and BMZ, were prepared by a two-step hydrothermal crystallization process, in which zeolite I synthesized in the first step is taken as a closed system and serves as the silicon sources for the growth of zeolite II crystals. The samples were defined as follows:

Composite BZZ: Just as the formers, Beta was the component of the composite as zeolite I and ZSM5 play zeolite II.

Composite BMZ: The composite was made up of Beta and MOR where Beta acted as zeolite I and MOR as zeolite II.

The samples were exchanged with 0.5 M NH_4NO_3 solution at room temperature and washed with deionized water. After drying, the samples were calcined at 550 °C for 3 h to form H-type zeolite. All the samples were ion-exchanged through 0.01 M $Co(OAc)_2$ to form CoH-zeolite. After it, they were calcined at 550 °C and crushed and sieved to 40-60 mesh granules.

The composites catalysts have hierarchically porous structures and tunable acidities. A series of information about zeolite composites have been reported[20]. It is also a promising support for NO-SCR since these properties and still need deeply study in this area.

General procedure: The catalytic reaction was performed in a quartz tube reactor with a mixture of NO, CH_4, O_2 and He (NO 2180 ppm, CH_4 2050 ppm, O_2 2 %, H_2O 2.5 %, He balance, GHSV = 7500 h^{-1}) fed over the catalyst. A gas-chromatograph with a TCD detector was used to analyze the exit gases.

Detection method: H_2-TPR experiments were carried out using a SORPTMATIC 1990 instrument. The catalysts were pretreated in air for 0.5 h at 550 °C. After cooling to room temperature, 10 % H_2/Ar (50 mL/min) was introduced in the system and the temperature was increased to 850 °C at a heating rate of 10 °C/min. The consumption of H_2 was analyzed with a thermal conductivity detector (TCD).

DRS (DRS-UV-visible) spectra of the Cary 300 apparatus UV-visible diffuse reflectance measurement instrument on the scanning range of 200-800 nm, slit width of 2 nm, scanning speed 600 nm/min.

NO-TPD was treated as follows: Firstly, 0.1 g of catalyst was packed in the reactor. Secondly, the catalysts activated by purging with highly purified He at 550 for 1 h and then cooled down to the room temperature for subsequent experiments. Thirdly, NO adopted with containing gas flow (50 mL/min) passed through the catalyst bed. Finally, the composition of the effluent gas was analyzed by a flue gas analyzer.

The infrared FT-IR spectrum of the sample is recorded in the region 4000-400 cm^{-1} in evacuation mode using KBr pellet technique with 1 cm^{-1} resolution on a SHIMADZU FTIR-Affinity-1 spectrophotometer.

The FTIR spectrometer SHIMADZU FTIR-Affinity-1 was also used with a DTGS KBr detector and a vacuum cell with CaF_2 windows attached to the vacuum apparatus and dosing system for pyridine adsorption. 20 mg of sample was *in situ* activated in the infrared pool for 2 h at 400 °C, when the temperature dropped to room temperature infrared spectra were recorded and then pass into the alkaline pyridine infrared pool, saturated adsorption. Finally, desorption of pyridine was performed at 3×10^{-3} Pa of pressure and the IR spectra were recorded at various temperatures to determine L acid and B acid.

$NO/O_2/CH_4$ adsorbed *in situ* IR profiles were characterized as follows: 15 mg of the solid acid catalyst samples, after grinding tablet, were *in situ* activated in the infrared pool for 2 h at 400 °C. When the temperature dropped to room temperature, it was recorded after the IR. Then, IR probe molecule NO + O_2 + CH_4 was introduced into the cell at 100 °C until the saturated adsorption was reached. Finally, desorption was performed at 3 of pressure at different temperatures *in situ* analysis by infrared spectroscopy.

X-ray photoelectron spectroscopy (XPS) measurements were performed with a hemispherical analyzer (SES R4000, Gammadata Scienta) using AlK_α (1486.6 eV) radiation. The pressure in the XPS chamber was around 10^{-9} mbar. The power of the X-ray source was 300 W and the energy pass for analyzer was 70 eV. The powder samples were pressed into indium foil and mounted on a special holder. The binding energy (BE) for Si, O and Co was measured by taking the C1s peak at 285 eV as internal standard, with an error of ± 0.2 eV for binding energy values. Before recording XPS, the catalysts were evacuated at 10^{-9} mbar in the XPS analyzer chamber. All spectra were fitted with a Voigt function (a composition 70/30 of Gaussian and Lorentz function) in order to determine the number of components under each XPS peak.

RESULTS AND DISCUSSION

Fig. 1 gave the NO conversion for CoH-BZZ and CoH-Beta under dry condition at a given temperature (550 °C). The maximum initial NO conversion to N_2 under dry conditions was 40 % over the CoH-Beta, so were 60 % over CoH-BZZ and 71 % over CoH-BMZ. The NO conversion on CoH-BZZ maintained within the range 56-60 % upon aged for 140 h under reaction in dry conditions. While, the catalyst CoH-BMZ showed a lower durability under the similar ageing procedures. CoH-Beta displayed one continuous decline range from 40 to 30 % in the same condition. Hence, it was found that CoH-BZZ expressed the best stability in dry feeds. Moreover, both CoH-BZZ and CoH-BMZ hadn't taken the appearance of byproducts in this process, such as N_2O, which expressed good selectivity of NO to N_2.

To determine the deactivation process under wet condition, the catalysts were kept on stream for 40 h at 550 °C. The reactant stream contained 2180 ppm of NO, 2050 ppm of CH_4, 2 % O_2 and 2.5 % H_2O in He. When introducing of

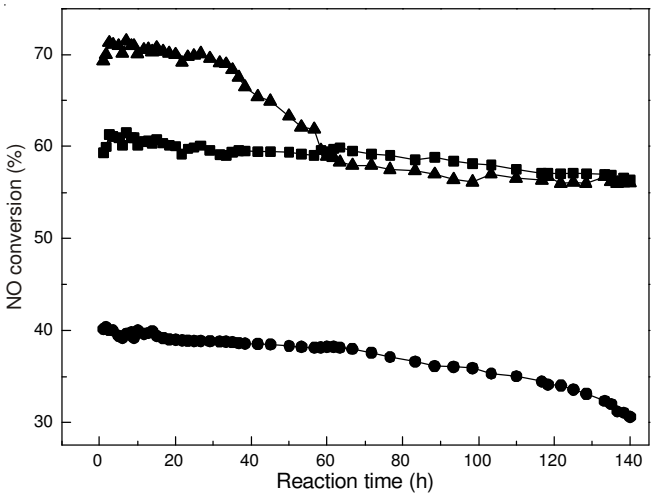

Fig. 1. NO conversion at 550 °C under dry condition, ■ CoH-BZZ, ▲ CoH-BMZ and ● CoH-Beta

water in the feeds, the activity of the catalyst decreased with different levels. CoH-BZZ was the good catalyst and the duplicate assay exhibited the same behavior. In this process, the activity of CoH-BZZ decreased from 60 to 38 % (Fig. 2b), while the one declined from 71 to 46 % for CoH-BMZ. The catalytic activity of CoH-Beta resulted in 23 % for NO conversion when in wet feed 1 h later. Simultaneously, the methane conversion (Fig. 2B) also got decreased over all of the catalysts in the same conditions. The amounts of NO conversion decreasing were 22 % over CoH-BZZ, 25 % over CoH-BMZ and 17 % over CoH-Beta under wet condition. Interestingly, the activity got back to the initial values well nigh after the vapor out of feed. In all the test samples, it began to recover easier over CoH-Beta just soon after the moisture atmosphere off. But it was beginning to recover over CoH-BZZ and CoH-BMZ 2 h later when the vapor was out. It could be seen that the coordination of H_2O and active site on composites based catalysts was more stable than on CoH-Beta. In another word, the activities on CoH-composites catalysts were harder to restore than it was on CoH-Beta. But all the composites based catalysts expressed superior water tolerance than CoH-Beta because of large amounts of active sites located.

Fig. 3 depicted the catalytic activity at different temperatures under wet condition over CoH-Beta and CoH-composites (-BZZ). As seen, the maximum NO conversions come with

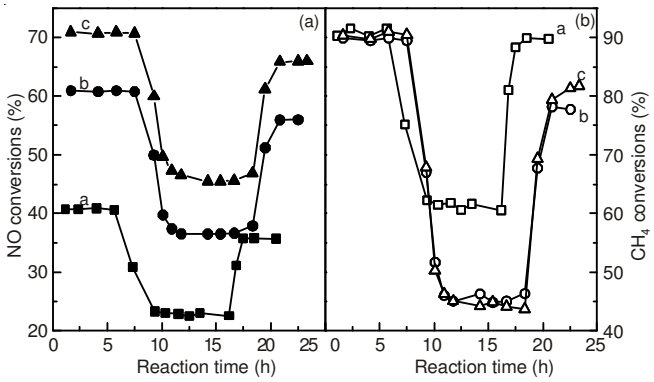

Fig. 2. Variation of NO and CH_4 conversions with time-on-stream for CoH-Beta (a) ,CoH-BZZ (b) and CoH-BMZ (c). T = 550 °C and 2.5 % of H_2O in the feeds

the temperature going up to 600 °C. It could also be seen that CH_4 combusted with O_2 more and the selectivity of NO to N_2 decreased with the reaction temperature above 600 °C. The maximum NO conversion over CoH-BZZ was 30 % compared with 23 % over CoH-Beta. However, it was 60 and 40 % of the NO conversion over CoH-BZZ and CoH-Beta under dry condition. Thus, the reactivity between these two samples was nearer under wet condition than the one under dry condition. In another word, the NO conversion of CoH-BZZ declined more in the presence of water.

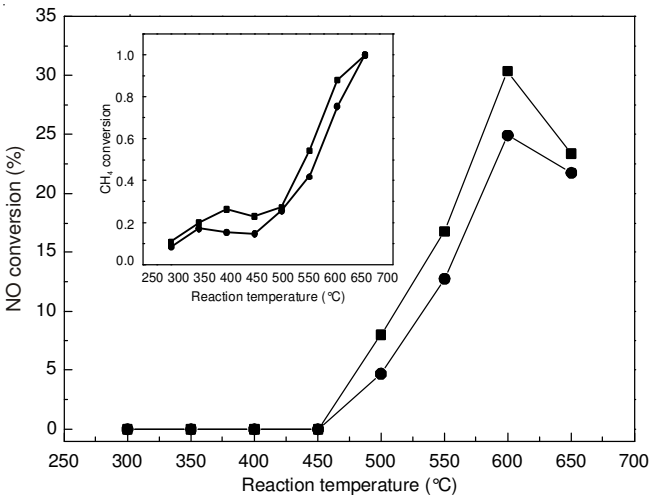

Fig. 3. Variation of NO and CH_4 conversions with temperature-on-stream (2.5 % H_2O) for CoH-BZZ ■ and CoH-Beta ●

In order to characterize the difference of fresh and deactivated samples, H_2-TPR was used and the profiles were shown in Fig. 4. Based on our results and on previous assignments in the literature[21], we allocated the reduction of Co species as follows: At 200 to 400 °C: reduction of Co oxide species like Co_3O_4 located outside of the zeolite pore structure. At 400 to 650 °C: reduction of Co-oxo species sited inside the zeolite channel. Above 650 °C: reduction of bare Co^{2+} bound to exchange sites of the zeolite.

The fresh sample of CoH-Beta expressed one shoulder peak from 200 to 650 °C and another peak at 850 °C. It can be due to the presence of multiple species of Co on the surface of

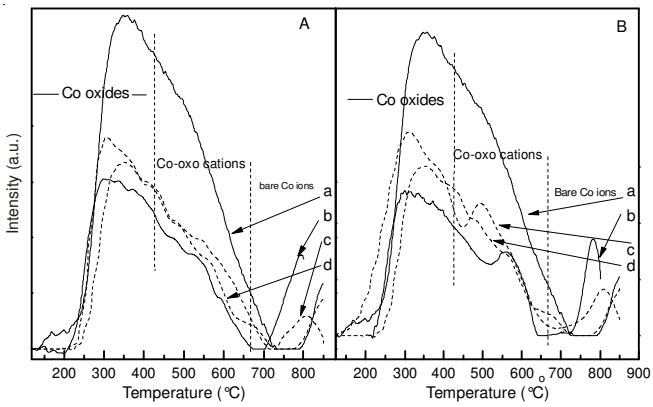

Fig. 4. H_2-TPR profiles of section A: fresh CoH-Beta(a), fresh CoH-BZZ(b), deactivated CoH-BZZ(c) and deactivated CoH-Beta(d); section B: fresh CoH-Beta(a), fresh CoH-BMZ(b), deactivated CoH-BMZ(c) and deactivated CoH-Beta(d)

catalyst. Fresh CoH-BZZ showed the reduction from 200 to 650 °C in all the test samples with low intensity. However, the bare Co^{2+} on CoH-BZZ was easier to reduce, which described respectively at 790 °C, compared with the one at 850 °C on CoH-Beta. CoH-BMZ (Fig. 4 Ab) and CoH-BZZ (Fig. 4Bb) show similar H_2-TPR patterns.

It was noteworthy that the Co^{2+} reduction peak of the test samples shifted to higher temperature when deactivated in the presence of vapor. For example, it switched from 790 to 815 °C for the deactivation sample CoH-composites (-BZZ and -BMZ) (Fig. 4d) compared with the fresh one (Fig. 4b). In contrast, the reduction peak from 200 to 650 °C was a little more intensive on deactivated samples than on fresh one. Thus, it can be seen that more amounts of cobalt oxide species sited on deactivation CoH-composites, which formation by the migration of partly bare Co^{2+}. CoH-Beta, on a contrary, obtained opposite result compared with CoH-composites. The inactivation sample displayed poor reduction from 200 to 650 °C compared with the fresh one. This could be speculated that some Co oxide species outflowed in the reaction because of the less stable properties. It must be noted that wet condition made poor effect on the less active Co^{2+} on CoH-Beta which possessed fewer Co^{2+} site. Nevertheless, it also played a more important role in the migration of Co^{2+} ions as well as in the growth of Co-oxo on CoH-BZZ and -BMZ.

The temperature-programmed desorption behavior of NO (NO-TPD) on the CoH-Beta and -BZZ was shown in Fig. 5. The profiles of the samples showed not only the NO desorption peak but also a heavy NO_2 one. This behavior may be due to the presence of some of NO interaction with O_2 remaining on the Co-oxo species in the zeolitic matrix. It was shown that CoH-BZZ had two types of adsorption centers, as signaled by two distinguished desorption peaks. Differently, there was only one peak on CoH-beta. Moreover, NO/Co and NO_2/Co ratio increased when the support was composites (BZZ) compared with Beta. The results were shown in Table-1.

TABLE-1
ADSORPTION AMOUNTS OF NO AND NO_2 PER MOLE OF Co^{2+} CATIONS ON THE VARIOUS CATALYSTS

Catalysts	NO/Co	NO_2/Co
CoH-Beta	1.83	48.55
CoH-BZZ	3.14	55.91

According to Dedecek *et al.*[22], the quartet bands at 650, 610, 580, 560 and 480 nm are attributed to β-type Co^{2+} ions, whereas the doublet bands at 510 and 540 nm characterize for γ-type Co ions. As for α-type Co^{2+} ions, the representative band should be near 685 nm, which was different in the prepared samples. The Co-oxo species could be characterized from 250 to 340 nm as suggested by Tabata *et al.*[23]. The spectra of other composites were similar to that of these samples. The bands above 700 nm could due to the Co oxide species over the surface of catalysts, such as Co^3O^4. UV-visible results (Fig. 6) indicated that more β- and α-type bare Co^{2+} ions and less Co-oxo cations and Co oxide species obtained on CoH-composites (-BZZ and -BMZ) than on CoH-Beta. As deactivation occurs, Co evolves from bare Co^{2+} ions to a mixture of CoOx moieties. The formation of oxide species decreased the number

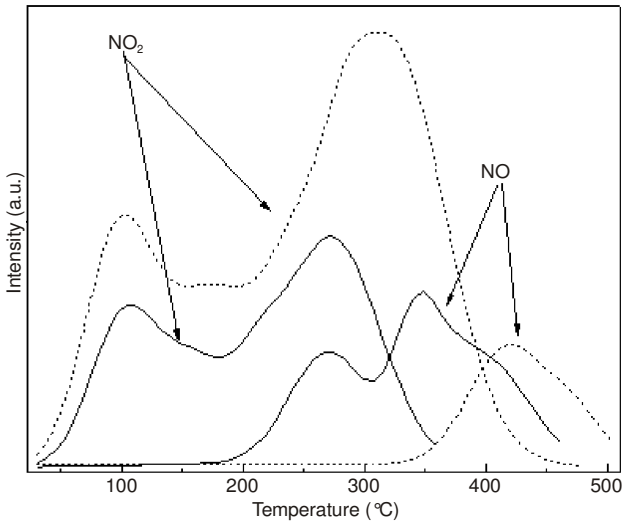

Fig. 5. NO TPD profiles of CoH-BZZ (solid line) and CoH-Beta (dash line) with the adsorption conducted at room temperature

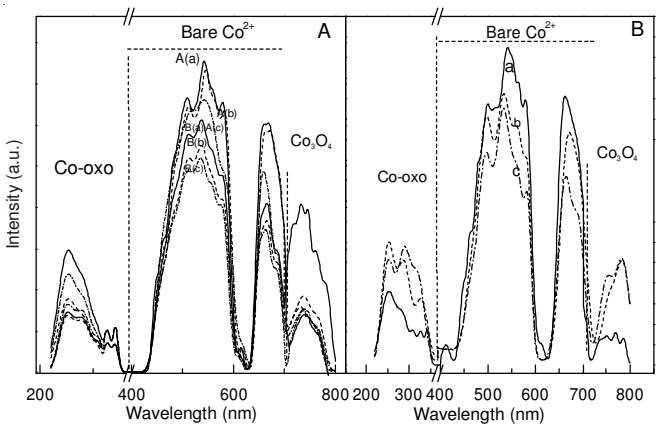

Fig. 6. UV-visible spectra of section A: A(a), fresh CoH-BZZ; A(b), spent CoH-BZZ after 140 h reaction in dry condition; A (c), deactivated CoH-BZZ under wet condition; B (a), fresh CoH-Beta; B (b), spent CoH-Beta after 140 h reaction in dry condition; B (c), deactivated CoH-Beta under wet condition; section B: a, fresh CoH-BMZ; b, spent CoH-BMZ after 140 h reaction in dry condition; c, deactivated CoH-BMZ under wet condition

of Co^{2+} active sites, hence lowering the global catalytic activity. It should be noted that there was still a fraction of bare Co^{2+} present in the three deactivated catalysts, presumably active in the reduction of NO_x, *albeit* at a much lower level than in the fresh samples. These results agree with literature reports for the catalytic performance of Co^{2+}-exchanged zeolites.

Fig. 7 depicted the FTIR spectra of chemisorbed pyridine in CoH-Beta and CoH-composites (-BZZ and -BMZ) (samples with fresh and deactivated) after subtraction of the spectrum of the pure activated sample. All the samples showed more Lewis acidity than Brönsted ones, while the formation of pyridinium ions on Brönsted acid sites exhibited the signals at 1549-1555 cm^{-1}, the pyridine coordinated to Lewis acid centers exhibits signals around 1450-1446 cm^{-1}. And the band at 1492 cm^{-1} is common to both types of sites. As expected, the sample deactivated CoH-composites (-BZZ and -BMZ) expressed lower intensity for Lewis acid than the fresh sample one. Interestingly, the strength of the Lewis site of deactivated CoH-composites (-BZZ and -BMZ) was just the same like the one

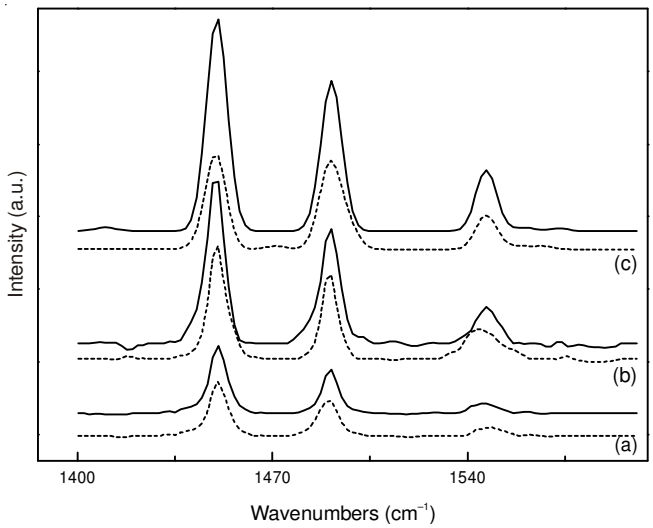

Fig. 7. FT-IR spectra of pyridine adsorbed on fresh (solid line) and deactivated samples (dash line) in the presence of vapor [CoH-Beta (a), CoH-BZZ (b) and CoH-BMZ (c)]

of fresh CoH-Beta. This must be based of more active Co ion-exchanged site presented in the composite which lead to the boost of the Lewis acidity. Yet, it was the chemisorption of H_2O on bare Co^{2+} sites which made the decline of Lewis acid.

Fig. 8 described the *in situ* IR profiles of adsorbed NO/O_2/CH_4 molecules on CoH-Beta and CoH-composites (-BZZ and -BMZ) with fresh and deactivated samples after adsorption at 100 °C and desorption at 400 °C, respectively. As seen, nitrates (1644 cm^{-1}) forms were found disappeared in significant amounts on the surface of deactivated CoH-Beta compared with the ones on fresh samples, so were the species Co^{2+}-$(NO)_2$ and -(NO) (1887 and 1985 cm^{-1})[24,25]. However, the species Co^{2+}-$(NO)_2$ and -(NO) were more intensities, while C=N (2330 cm^{-1}) intermediates absented on the deactivated sample of CoH-composites (-BZZ and -BMZ). C=N was considered to be the main intermediates and obviously formed on the fresh ones (Fig. 8). Moreover, the intensity order of the intermediates species can match with the catalytic activity well, in which the deactivated CoH-Beta worked as the worst of them.

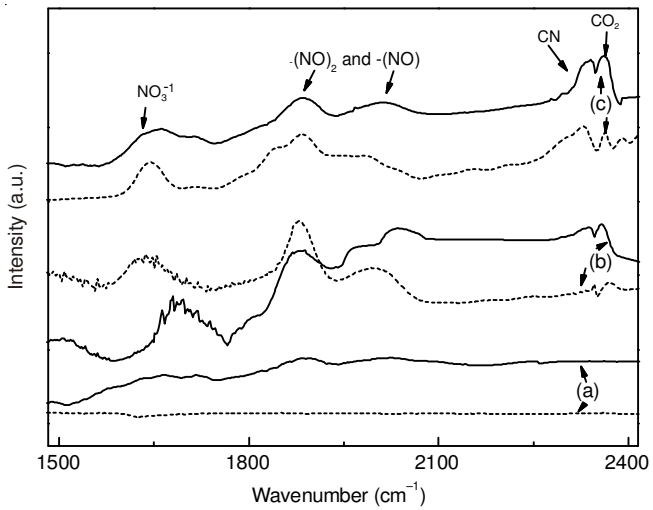

Fig. 8. FT-IR spectra of NO/O_2/CH_4 adsorbed over fresh (solid line) and deactivated samples (dash line) in the presence of vapor (CoH-Beta (a), CoH-BZZ (b) and CoH-BMZ (c)

The FT-IR spectra of the composites are shown in Fig. 9, in which the characteristic vibration bands of silica-alumina zeolite can be observed, although the bands position and intensity are not completely identical. The bands around 1069 and 459 cm^{-1} are assigned to the anti-symmetric stretching vibrations and the O-T (Si or Al) bending vibrations of zeolite, respectively and the band around 576 cm^{-1} can be ascribed to five member ring vibrations. The bands around 1000, 465 and 570 cm^{-1} are attributed to T-O-T anti-symmetric stretching vibrations, the O-T (Si or Al) bending vibrations, respectively. It can be shown from Fig. 9 that the bands between 1100 and 1060 cm^{-1} appeared obviously, which was at 1070 cm^{-1} for CoH-Beta, at 1084 cm^{-1} for CoH-BMZ and at 1094 cm^{-1} for CoH-BZZ.

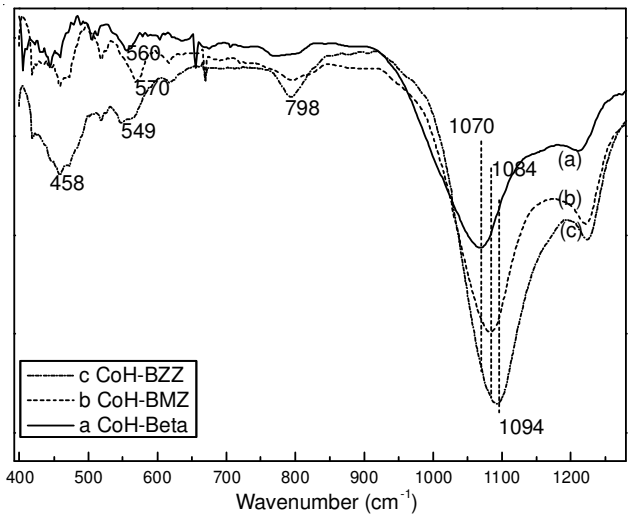

Fig. 9. IR spectra of zeolites

XPS measurements of fresh (as prepared) or deactived (just after catalytic test and conditioned in a wet flowing air at 550 °C for 3 h) CoH-Beta and CoH-composites (-BZZ and -BMZ) were analyzed in the binding energy regions of Si2p, Al2p, Co2p, O1s.and C1s.

The Si2p binding energy value (103.6 eV) on BZZ and (103.2 eV) on BMZ close to that reported earlier for BEA, MFI and MOR zeolites[26], is related to the presence of tetrahedral Si(IV). The O 1s line can be decomposed into three components: a main peak at 533.1 eV was assigned to oxygen of the zeolite framework, a smaller peak (2-3 % of the total O 1s intensity) at 530.7 eV due to oxygen-metal bonds[27].

A main contribution of C 1s spectra is located at binding energy of about 285.0 eV. This peak can be assigned to adventitious carbon[28]. The adventitious carbon on the sample surface may originate from atmosphere, sample handling or contamination in the XPS chamber. The distinct peak at 281.2 eV corresponds to deposited carbon species of the graphite type which appeared after the catalyst CoH-Beta was used, but it disappeared on the CoH-composites after used.

The Co 2p core level spectrum is characterized by two components, by which due to spin-orbital splitting-Co 2p3/2 and Co 2p1/2 and shake-up satellites. As shown in Fig. 10a, for CoH-Beta, the Co 2p3/2 doublet is at 783.3 eV and the second at 789.3 eV; the Co 2p1/2 doublet is at 799.2 eV and the satellite at 805.1 eV[26,29].

Another one with a binding energy around 778.6 eV; this state of cobalt is attributed to the cobalt oxides (CoO or Co_3O_4)[28,30,31], the presence of Co oxides in CoH-Beta is confirmed by the charge transfer satellite of Co $2p_{3/2}$ at 783 eV and of Co $2p_{1/2}$ at 799.2 eV and by the value of the Co $2p_{3/2}$-Co $2p_{1/2}$ splittings of 15.9 eV[29].

It is important to underline that for CoH-composites catalysts the two value of binding energy of $Co2p_{3/2}$ and $Co2p_{1/2}$ are at 782.7 and 799.1 eV in CoH-BZZ and at 782.6 and 799.1 eV in CoH-BMZ, which are lower than CoH-Beta.

The corresponding difference supports prepared catalysts shows that some impact on the binding energy of Co. It should be noted that the appearance of Co^{3+} is less on CoH-BZZ.

However, CoO or Co_3O_4 and Co^{2+} co-existing in the presence of CoH-zeolites, which is more apparent on CoH-Beta than on CoH-BZZ. Furthermore, we have found in our previous

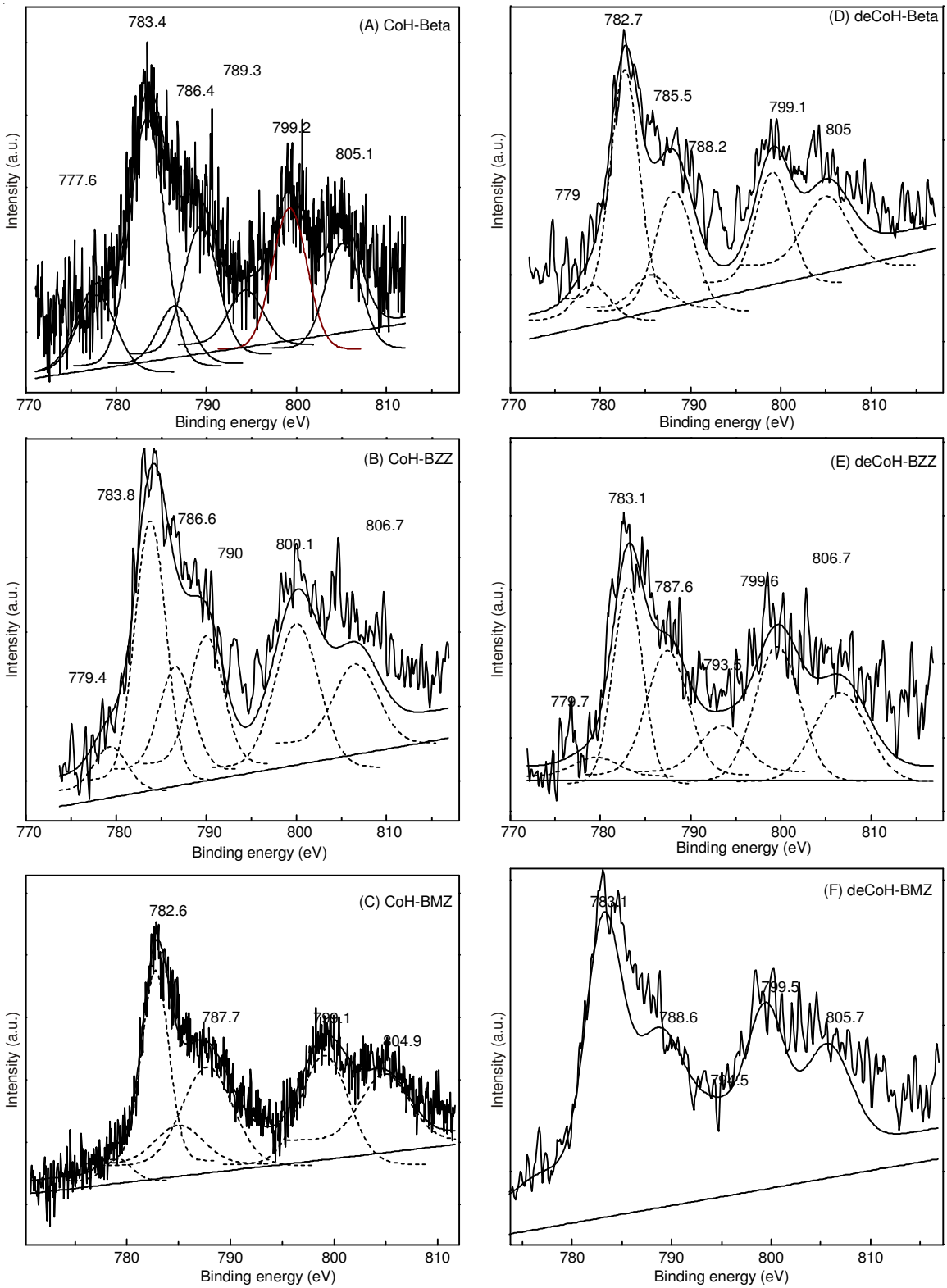

Fig.10. XPS pattern of Co2p on various catalysts

study that Co^{2+} ion is the most active species and cobalt oxide has lower activity for SCR of NO than Co^{2+}. Hence, the coexistence of Co^{2+} ions and cobalt oxides in catalysts CoH-Beta have decreased the percentage amount of Co^{2+} ions and the activity as compared to catalysts CoH-composites, which have more Co^{2+} ions. After deactivation in the presence of vapor, it can be noted that the binding energy of $Co2p_{3/2}$ in CoH-BZZ are differed from 782.3 to 783.1 eV (Fig. 10B and E). Similar tendency occurred on CoH-Beta (Fig.10 A and D), while it also show a decrease of the exposure of cobalt (Table-2). Thus, the catalyst CoH-BZZ do show a significant change in the dispersion of cobalt from Co^{2+} to CoO after its use in the reaction in the presence of vapor, which because a small binding energy value at 779.7 occurred. These XPS results confirm that the ion-exchange method produces cobalt species mainly as Co^{2+} ions, which are the most active catalytic sites for CH_4-SCR of NO.

In present work, the effect of supports on Co-based catalysts in NO-SCR was studied through the characterization of physico-chemical properties of the catalysts and the reactivity in the absence or presence of vapor.

It is seen that large effect of supports on the properties, such as active sites binding energies and adsorption energies, of catalysts. CoH-BZZ and CoH-BMZ composites catalysts are expected with some special properties which lead the CH_4 selective reduction of NO to N_2.

The zeolite binding energies are seen to shift in a regular progressive fashion with changes in the [Si/Al] ratio[30]. The difference in binding energies of Si(2p) and Al(2p) can be rationalized by an increased charge on the zeolite framework upon substituting Si for Al, of which leads to an unequal charge distribution in SiO_4 and AlO_4 units. For Al-O bond, the one to the oxygen with the unpaired electron increases considerably, while the other three distances would slightly decrease. Thus, the reduction of the aluminum content in the zeolite system, *i.e.*, HZSM5-HBeta- HMordenite -HY, results in a continued increase in the covalent influence of the Al--O bond, with continuous decrease in binding energy of O(ls). So was the XPS results of CoH-BMZ which binding energy was lowest among all the catalysts. However, the relatively high Si/Al ratio, but similar binding energy of Si, Al and O in the composite BZZ compared with Beta could be caused by follows. For CoH-BZZ, some Si-O-Si and Si-O-Al bonds in the BEA and MFI the destructed and several additional AlOH groups formed at the interface of two topologies. It can then be noted that the oxygens shared by Al and Si atoms in BZZ and BMZ were more effectively polarized. The bond between the silicon and oxygen was made more covalent than it was with just (structural) ZSM5, MOR and Beta present. In another word, the polarization boosted the generation of the electron hole produces substantial geometry relaxation[29].

As the skeleton FT-IR spectra expressed, the broad and high intensity anti-symmetric stretching band of the unperturbed T-O-T bonds characterized at about 1094,1084 and 1070 cm^{-1} for CoH-BZZ, -BMZ and -Beta. Obviously, the cation-framework oxygen bonding should parallel the stability of similar oxygen ligand complexes, but an additional effect of confinement of the complex in the electric field of the zeolite channels cannot be omitted. Considered by the vibration frequency formula $\nu = \sqrt{k/\mu/2\pi}$ [32], framework vibration bands shift to higher frequency was the result of short Al-O bond length and forced bond constants. In this last case, the value of the frequency shift (relaxation shift) correlated with the strength of the cobalt-ligand interaction well. The value of a shift, using for convenience the position of the unperturbed T-O-T anti-symmetric stretching band in hydrated sample as reference, was related to the change of the T-O-T angle and the degree of the local deformation of the lattice caused by the vicinity of the divalent cation[33]. Then, it was the stronger polarization of zeolitic oxygen atoms generated which induces long-range electrostatic[34]. The zeolite crystal long-range electrostatic contributions had been shown to play a non-negligible part in differences in stabilization energies of cationic transition states.

Long-range effects[34] of the zeolite framework stabilize the positively charged electron hole defect. As a result, there was a corresponding progressive increase in the ionicity (relative acidity) of the H--O bonds in BZZ and BMZ, so were the Co^{2+} ions sites. XPS results confirm that the cobalt species produced by ion-exchange method on CoH-BZZ and CoH-BMZ mainly as Co^{2+} ions (Fig.10 b and c) and they have lower relative binding energy than the ones on CoH-Beta.

The results of low binding energy on CoH-composites (-BZZ and -BMZ) with further stronger adsorption capacity were considered. The intermediates of NO on bare Co^{2+} ions was considered to be as Co^{2+}-$(NO)_2$ and Co^{2+}-(NO) (Fig. 8), which was heavier appeared on CoH-composites than on CoH-Beta. It was also approved by the NO-TPD results that stronger adsorption of NO on per active sites expressed on CoH-BZZ (Table-1). And desorption of NO_2 due to the intermediates NO_3^- on Co-oxo species, which was also more powerful on CoH-composites.

It is reported that the differences of Al/Si substitution energies and the adsorption energies related to the site of Al substitution and the site at the intersection of two channels were considered to have the lowest substitution energies[35]. To clarify the two different adsorption sites of BZZ and BMZ, we identified the binding energies of Co^{2+} ions to the BZZ and BMZ framework.

TABLE-2
XPS DATA OF PREPARED CATALYSTS

	Si/Al	Co/Al	Si2p	Al2p	O1s	C1s	Co (wt. %)
CoH-Beta	17.5	0.53	103.6	75.2	532.8	284.8	2.4
CoH-BZZ	37.95	0.56	103.7	74.6	532.9	284.7	2.2
CoH-BMZ	12.26	0.32	103.2	74.2	532.5	284.5	2.2
CoH-deBeta	17.5	0.46	103.7	75.3	532.9	284.9	2.0
CoH-deBZZ	37.95	0.56	103.7	75.0	532.8	284.7	2.2
CoH-deBMZ	12.26	0.31	103.5	74.8	532.8	284.7	2.2

The Co^{2+} binding sites were classified according to their location in the BZZ and BMZ framework, in the perpendicular channel. Three different types of the Co^{2+} [5] binding sites were found: (i) the Co^{2+} ion located on the intersection of two channels interacts only with four oxygen atoms of the AlO_4 tetrahedron, which defined as α-type bare Co^{2+}; (ii) the Co^{2+} ion located in the main channel interacts with oxygen atoms of five- or six-membered ring containing aluminum, which defined as β-type bare Co^{2+} ions and (iii) the Co^{2+} ion interacts with oxygen atoms belonging to more than one ring. The relative stabilities of the individual α-type Co^{2+} binding sites depend on the position of the Al atom. As depicted that more β- and α-type bare Co^{2+} ions and less Co-oxo cations and Co oxide species obtained on CoH-composites, better NO conversion on CoH-composites than on CoH-Beta expressed. These results point out again to the role of bare Co^{2+} ions (β- and α-type), which were considered to be the two sites with different substitution energies and worked as two obvious adsorption site and active sites of the catalysts in this reaction. The speciation of Co in Co-zeolites investigated in this work allows to proof that the "structure-properties" relationship in the SCR of NO by CH_4 was important.

It could be seen clearly that more powerful stability for CoH-BZZ compared with CoH-Beta under dry condition for 140 h (Fig. 1). As UV characterized, the intensity of the active sites bands declined a little with different degrees on spent ones, which expressed more visible on CoH-Beta than on CoH-composites (-BZZ and -BMZ). The impacts of active sites stability by supports were then been confirmed and steadier Co^{2+} located on CoH-BZZ than on CoH-beta could be speculated.

Based on the above observations, the results reported earlier indicate that the support strongly influenced the thermal stability of SCR catalysts. The ageing treatments modify the surface cobalt species and the support influencing both the activity and the stability for the reduction of NO_x by CH_4. According to the literatures[36], the activity loss of cobalt zeolites under rigorous reaction conditions is generally believed to be related to redistribution of cobalt species. Firstly, the decrease in the NO_x conversion with respect to the CoH-Beta ageing in dry feeds can be attributed to the loss of the active sites, which because of a lower polarization of Co cationic states and zeolitic oxygen atoms. Secondly, an issue to be considered is the good stable catalytic behavior of CoH-BZZ, which can attribute to the stronger polarization and long-range effects. However, it was the too effective active sites to bring out easier migration from Co^{2+} to Co oxide on CoH-BMZ, which lead to less stability.

In a comprehensive overview of SCR of NO_x with hydrocarbons, it was stressed that the need for tests on the time-on-stream behavior of metal-loaded zeolites in real exhaust gas for a good evaluation of their potential for practical application. In this respect, the presence of water in the test conditions is a prerequisite. Supports took key impact on the catalysts properties in this process.

Under wet condition, CoH-composites (-BZZ and -BMZ) expressed improved NO conversion than CoH-Beta. On contrary, the CH_4 conversions under wet condition were not advanced over CoH-composites, which was 50 % over CoH-BZZ and 45 % over CoH-BMZ compared with 60 % over CoH-Beta. Thus, superior selectivity for CoH-composites in the reaction under wet condition was done obviously. After water extracting from the feeds, both the conversions of NO and CH_4 made recoveries to close in the initial values with different degrees. In between, the values on CoH-composites were closer to the initials, which is due to the better stability of active sites. Better CH_4 conversion recovery ability occurred on CoH-Beta than on CoH- composites due to the combustion of CH_4 on Co oxide species. And partly loss of NO conversion after wet condition owing to the transformation of few part of bare Co^{2+} in wet feeds, as clearly reported[25]. It was further approved by H_2-TPR that the oxide species decreased a lot on CoH-Beta after deactivation in wet feed (Fig. 4). Thus, it could be due to the outflow of few active sites on CoH-Beta to lead to the decrease of activity after timing wet feed reaction. However, CoH-BZZ worked more stable at this process with more fixed active sites locating.

Water is the smallest molecules among all the feeds, it can more easily diffuse and adsorb on the active sites. Thus, under wet condition, it must be the introduction of H_2O to the feed stream of our reactor caused a sharp drop of adsorption of NO and CH_4, which is due to the competitive adsorption of H_2O, NO and CH_4 on the Co^{2+} sites of the catalysts. And the active sites on CoH-composites were more vivacious, which lead sharper competitive adsorption among H_2O, NO and CH_4. As a result, NO conversion decreased 22 % under wet condition over CoH-BZZ and 25 % over CoH-BMZ. On contrary, the NO conversion declined 17 % over CoH-Beta in the same process. Considered from these, H_2O adsorbed more on the active site of CoH-composites than CoH-Beta. It also got a more fixed coordination with exchanged Co^{2+} of CoH- composites with a result in longer recovery time for catalytic activity after water extracting from the reaction feeds (more than 1 h later when the catalytic activity began to recover over CoH-composites compared with the recovery of CoH-Beta just soon after water was extracted from the feeds) (Fig. 2). However, it was more exchanged bare Co^{2+} sited on the CoH-BZZ and CoH-BMZ, which bring out the higher NO conversions (37 and 45 %) compared with the one (23 %) on CoH-Beta.

Characterization by XPS allowed correlating the different structural modifications observed for catalysts with various supports with the different changes of their Co bind energy, which results in various Lewis acid and adsorption ability.

As pyridine adsorbed IR characterized, the Lewis acid in the sample deactivated CoH-composites (-BZZ and -BMZ) decreased compared with the one in the fresh sample, which following confirmed that water chemisorbed on the exchanged bare Co^{2+} under wet condition. According to the *in situ* IR profiles of adsorbed $NO/O_2/CH_4$ described, nitrates, Co^{2+}-(NO), -$(NO)_2$ and C=N species were considered to be the main intermediates, of which the intensity was stronger on the fresh samples than on the deactivated ones. Thus, the less intensity of intermediates on the deactivated sample should approve that water insist the activation of NO and CH_4, which result in the deactivation of the catalysts (Fig. 8). Furthermore, the strength of the Lewis site of deactivated CoH-composites (-BZZ and -BMZ) (Fig. 7) was still higher than the one of the fresh CoH-Beta. Interestingly, the NO conversions of both two samples got to around 40 %. Thus, Lewis acid was the key

point for NO-SCR, which affected by the chemi-adsorption of water in the reaction. Finally, CoH-BZZ expressed good per active site adsorption ability, but also possessed a stronger competitive adsorption between water and reactants, which need to be improved in the following.

Yet, it could then be deliberated that the deactivation for samples in this reaction was different for different supports and different reaction condition. The loss of active sites was the main reason for deactivation of NO-SCR with methane under dry condition, which was more serious on CoH-Beta. Moreover, the competitive adsorption of H_2O and reactants on bare Co^{2+} sites of the catalysts mainly lead to the deactivation in the presence of water vapor, which was more severe on CoH-composites.

Thereby, it must be pointed out here that the introduction of MFI or MOR to the BEA generated more defect sites and gave rise to an interface structure, which different from both zeolite Beta, MOR and MFI structures and generated entangle joint of these structures or a transition from bulk MFI and MOR structure to bulk Beta structure. The active Co located here with shorter distance between each other and the coordination O of different topology have different bond energies, resulting in stronger electric effect and synergetic effect. Some lower binding energy of Co 2p on CoH-composites improved more active properties expressed by stronger Lewis acid and adsorption ability, which result in higher reactivity of NO-SCR in the absence of vapor. But it also took more competitive adsorption among water and NO, which resulted in higher decline of NO conversion.

Conclusions

• The "structure-properties" relationship in the SCR of NO by CH_4 is investigated for CoH-Beta and CoH-Beta based composites (CoH-BZZ and CoH-BMZ) in this work by catalytic reaction in the absence and presence of vapor and other characterizations.

• It was shown that cobalt was incorporated into the BZZ and BMZ lattice as tetrahedral Co^{2+} ions with highly dispersion and low binding energy. Moreover, stronger electro polarization and long-range effect took a result in better acidity, adsorption and reaction on BZZ and BMZ supports.

• Upon ageing procedure for 140 h with dry feeds, CoH-BZZ expressed the best catalysis stability, but CoH-BMZ put the worst. Under wet condition, both CoH-BZZ and CoH-BMZ expressed better reactivity than CoH-Beta did. Further studies are undertaken to complement the competitive adsorption among H_2O, NO and CH_4 on exchanged bare Co^{2+} sites which play as the main deactivation mechanism under wet condition. More amounts and better redox active sites over CoH-composites were found to result in the stronger competitive adsorption between H_2O and reactant over CoH-BZZ than it did over CoH-Beta. Thus, the sharper decrease of NO conversion on CoH-BZZ for 22 % and on CoH-BMZ for 25 % compared with the one of 17 % on CoH-Beta existed.

• Furthermore, two deactivation reasons were being for NO-SCR by CH_4. Firstly, the loss of the active sites because of a lower polarization of Co cationic states and zeolitic oxygen atoms; secondly, the easier migration of active sites from Co^{2+} to Co oxide on account of more effective active sites. The deactivation of CoH-Beta was on behalf of the forward one and the one of CoH-BMZ result from the last one.

ACKNOWLEDGEMENTS

This work is supported by the National Science Foundation of China (NO. 20876102) and the Ministry of Education of China (NO. 200801120006).

REFERENCES

1. G. Busca, L. Lietti and F. Berti, *Appl. Catal. B*, **18**, 1 (1998).
2. J.H. Li, H.Z. Chang, L. Ma, J.M. Hao and R.T. Yang, *Catal. Today*, **175**, 147 (2011).
3. M. Shelef and G.W. Graham, *Catal. Rev. Sci. Eng.*, **36**, 443 (1994).
4. S.B. Kang, S.J. Han, S.B. Nam, I.-S. Nam, B.K. Cho, C.H. Kim and S.H. Oh, *Chem. Eng. J.*, **207-208**, 117 (2012).
5. J.N. Armor, *Catal. Today*, **26**, 147 (1995).
6. L. Capek, J. Dedecek and B. Wichterlová, *J. Catal.*, **227**, 352 (2004).
7. E. Ivanova, K. Hadjiivanov, D. Klissurski, M. Bevilacqua, T. Armaroli and G. Busca, *Micropor. Mesopor. Mater.*, **46**, 299 (2001).
8. Y. Hu, K. Griffiths and P.R. Norton, *Surf. Sci.*, **603**, 1740 (2009).
9. A. Boix, E.E. Miró, E.A. Lombardo, M.A. Bañares, R. Mariscal and J.L.G. Fierro, *J. Catal.*, **217**, 186 (2003).
10. M.A. Ulla, L. Gutierrez, E.A. Lombardo, F. Lónyi and J. Valyon, *Appl. Catal. A*, **277**, 227 (2004).
11. M. Muller, G. Harvey and R. Prins, *Micropor. Mesopor. Mater.*, **34**, 135 (2000).
12. M. Shelef, *Chem. Rev.*, **95**, 209 (1995).
13. P. Praserthdam, N. Mongkolsiri and P. Kanchanawanichkun, *Catal. Commun.*, **3**, 191 (2002).
14. M. Lezcano, A. Ribotta and E. Miró, *J. Catal.*, **168**, 511 (1997).
15. Y.J. Li, P.J. Battavio and J.N. Armor, *J. Catal.*, **142**, 561 (1993).
16. T.J. Lee, I.S. Nam, S.W. Ham, Y.-S. Baek and K.-H. Shin, *Appl. Catal. B*, **41**, 115 (2003).
17. Y.J. Li and J.N. Armor, *J. Catal.*, **150**, 376 (1994).
18. M. Ogura, S. Kage, T. Shimojo, J. Oba, M. Hayashi, M. Matsukata and E. Kikuchi, *J. Catal.*, **211**, 75 (2002).
19. C. Chupin, A. Vanveen, M. Konduru, J. Despres and C. Mirodatos, *J. Catal.*, **241**, 103 (2006).
20. J. Zheng, Y. Yi, W. Wang, K. Guo, J. Ma and R. Li, *Micropor. Mesopor. Mater.*, **171**, 44 (2013).
21. M.A. Ulla, L. Gutierrez, E.A. Lombardo, F. Lónyi and J. Valyon, *Appl. Catal. A*, **277**, 227 (2004).
22. J. Dedecek, D. Kaucký and B. Wichterlová, *J. Catal.*, **211**, 198 (2002).
23. T. Tabata, H. Ohtsuka, L.M.F. Sabatino and G. Bellussi, *Micropor. Mesopor. Mater.*, **21**, 517 (1998).
24. T. Montanari, M. Bevilacqua, C. Resini and G. Busca, *J. Phys. Chem. B*, **108**, 2120 (2004).
25. D. Pietrogiacomi, M.C. Campa and V. Indovina, *Catal. Today*, **155**, 192 (2010).
26. J. Janas, T. Machej, J. Gurgul, R.P. Socha, M. Che and S. Dzwigaj, *Appl. Catal. A*, **75**, 239 (2007).
27. L.P. Oleksenko, *Theor. Exp. Chem.*, **40**, 331 (2004).
28. A.V. Boix, S.G. Aspromonte and E.E. Miró, *Appl. Catal. A*, **341**, 26 (2008).
29. X. Solans-Monfort, V. Branchadell, M. Sodupe, M. Sierka and J. Sauer, *J. Chem. Phys.*, **121**, 6034 (2004).
30. H.H. Chen, S.C. Shen, X. Chen and S. Kawi, *Appl. Catal. B*, **50**, 37 (2004).
31. A.V. Boix, J.M. Zamaro, E.A. Lombardo and E.E. Miró, *Appl. Catal. B*, **46**, 121 (2003).
32. R. Szostak, *J. Catal.*, **101**, 549 (1986).
33. Z. Sobalík, Z. Tvaruzková and B. Wichterlová, *J. Phys. Chem. B*, **1029**, 1077 (1998).
34. N. Katada, K. Suzuki, T. Noda, G. Sastre and M. Niwa, *J. Phys. Chem. C*, **113**, 19208 (2009).
35. X.L. Sun, C.P. Huang, J.Zhang and B.-H. Chen, *Acta Phys.-Chim. Sin.*, **25**, 1136 (2009).
36. M.C. Campa, V. Indovina and D. Pietrogiacomi, *Appl. Catal. B*, **91**, 347 (2009).